S33

Upper Limits of Diffuse Gamma Rays from the Galactic Plane at 10 TeV with the Tibet-II and III Arrays

(The Tibet ASγ Collaboration)

M. Amenomori[1], S. Ayabe[2], S.H. Cui[3], Danzengloubu[4], L.K. Ding[3], X.H. Ding[4], C.F. Feng[5], Z.Y. Feng[6], X.Y. Gao[7], Q.X. Geng[7], H.W. Guo[4], M. He[5], K. Hibino[8], N. Hotta[9], H.B. Hu[3], J. Huang[9], Q. Huang[6], M. Izumi[11], H.Y. Jia[6], F. Kajino[11], K. Kasahara[12], Y. Katayose[13], K. Kawata[11], Labaciren[4], C.L. Lan[3], G.M. Le[14], J.Y. Li[5], H. Lu[3], S.L. Lu[3], X.R. Meng[4], K. Mizutani[2], J. Mu[7], H. Nanjo[1], M. Nishizawa[15], M. Ohnishi[10], I. Ohta[9], T. Ouchi[10], S. Ozawa[9], J.R. Ren[3], T. Saito[16], M. Sakata[11], T. Sasaki[8], M. Shibata[13], A. Shiomi[10], T. Shirai[8], H. Sugimoto[17], K. Taira[17], M. Takita[10], Y.H. Tan[3], N. Tateyama[8], S. Torii[8], H. Tsuchiya[10], S. Udo[2], T. Utsugi[8], B.S. Wang[3], H. Wang[3], Y.G. Wang[5], L. Xue[5], X.C. Yang[7], Y. Yamamoto[11], Z.H. Ye[14], G.C. Yu[6], A.F. Yuan[4], T. Yuda[18], H.M. Zhang[3], J.L. Zhang[3], N.J. Zhang[5], X.Y. Zhang[5], Zhaxisangzhu[4] and X.X. Zhou[6]

[1]Department of Physics, Hirosaki University, Hirosaki 036-8561, Japan

[2]Department of Physics, Saitama University, Saitama 338-8570, Japan

[3]Laboratory of Cosmic Ray and High Energy Astrophysics, Institute of High Energy Physics, Chinese Academy of Sciences, Beijing 100039, China

[4]Department of Mathematics and Physics, Tibet University, Lhasa 850000, China

[5]Department of Physics, Shandong University, Jinan 250100, China

[6]Institute of Modern Physics, South West Jiaotong University, Chengdu 610031, Chi na

[7]Department of Physics, Yunnan University, Kunming 650091, China

[8]Faculty of Engineering, Kanagawa University, Yokohama 221-8686, Japan

[9]Faculty of Education, Utsunomiya University, Utsunomiya 321-8505, Japan

[10]Institute for Cosmic Ray Research, University of Tokyo, Kashiwa 277-8582, Japan

[11]Department of Physics, Konan University, Kobe 658-8501, Japan

[12]Faculty of Systems Engineering, Shibaura Institute of Technology, Saitama 330-8570, Japan

[13]Faculty of Engineering, Yokohama National University, Yokohama 240-0067, Japan

[14]Center of Space Science and Application Research, Chinese Academy of Sciences, B eijing 100080, China

[15]National Institute for Informatics, Tokyo 112-8640, Japan

[16]Tokyo Metropolitan College of Aeronautical Engineering, Tokyo 116-0003, Japan

[17]Shonan Institute of Technology, Fujisawa 251-8511, Japan

[18]Solar-Terrestrial Environment Laboratory, Nagoya University, Nagoya 464-8601, Japan

ABSTRACT

Diffuse gamma rays from the Galactic plane have been searched using the combined data with the Tibet-II and III air shower arrays at energies around 10 TeV. The sky regions searched are the inner Galaxy, $20^\circ \leq l \leq 55^\circ$, and outer Galaxy, $140^\circ \leq l \leq 225^\circ$, and $|b| \leq 2^\circ$. No significant Galactic plane gamma-ray excess was observed. The 99% confidence level upper limits for gamma-ray intensity at 10 TeV obtained for $|b| \leq 2^\circ$ are 2.8×10^{-17} $\mathrm{cm^{-2}s^{-1}sr^{-1}MeV^{-1}}$ for the inner Galaxy, and 1.05×10^{-17} $\mathrm{cm^{-2}s^{-1}sr^{-1}MeV^{-1}}$ for the outer Galaxy, assuming a differential spectral index of 2.4. The present results give the most stringent upper limits on the inverse Compton model with a source electron spectral index of 2.0, even though compared to those from Cherenkov telescopes in the lower energy region and other air shower arrays in the higher energy region.

Yangbajing site (4300 m a.s.l., 90.5° E, 30.1° N) in Tibet, China

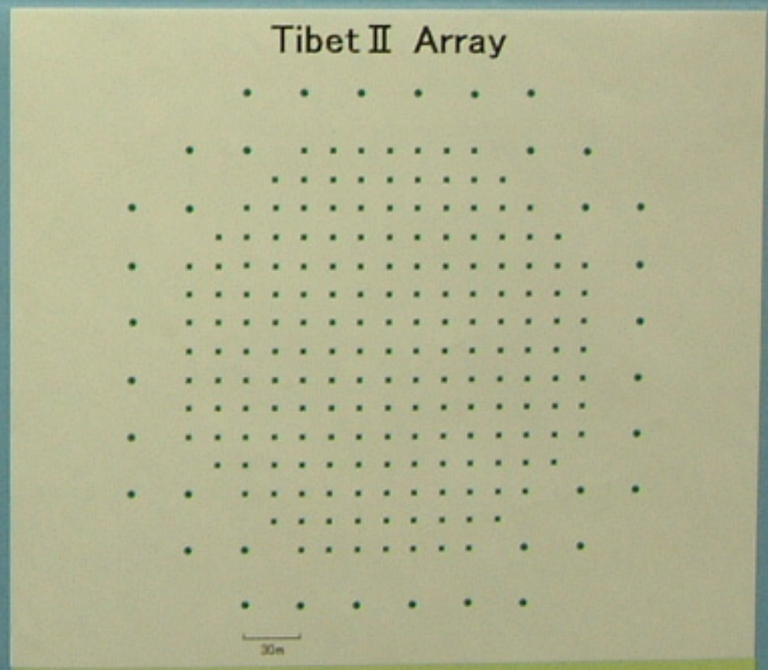

Fig. 1.— Map of the Tibet-II array at Yangbajing. Air shower events hitting the inner area with 15m detector distance are used in the analysis.

1. INTRODUCTION

A detailed intensity distribution of high-energy gamma rays coming from the Galactic plane was given by Hunter et al. (1997) based on EGRET observations. In the energy

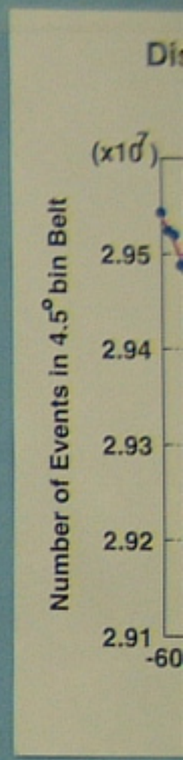

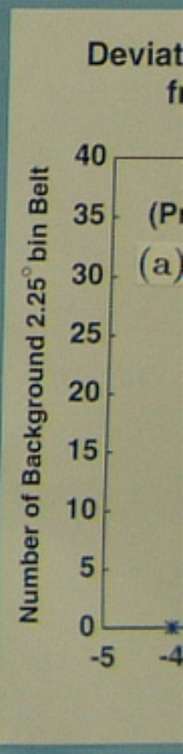

Galaxy, assuming a differential spectral index of 2.4. The present results give the most stringent upper limits on the inverse Compton model with a source electron spectral index of 2.0, even though compared to those from Cherenkov telescopes in the lower energy region and other air shower arrays in the higher energy region.

1. INTRODUCTION

A detailed intensity distribution of high-energy gamma rays coming from the Galactic plane was given by Hunter et al. (1997) based on EGRET observations. In the energy region above 1 GeV, the gamma-ray intensity from the inner Galaxy is higher than the COS B data by a factor of about 3. It is also higher than the conventional model predictions (e.g., Hunter et al. 1997; Bertsch et al. 1993) by a factor of 1.7, assuming the power law proton spectrum with spectral index of 2.75. Mori (1997) showed that the latter discrepancy can be interpreted by adopting a harder proton spectral index of 2.45 for the EGRET excess within a plane thickness of $|b| \leq 10°$. Webber (1999) also showed that the EGRET excess i n $|b| \leq 5°$ can be reproduced by assuming a source proton spectral index of 2.25.

Porter & Protheroe (1997) indicated that in such a high-energy region, cosmic-ray electrons may create a significant part of the diffuse gamma rays, depending on their injection spectral index and acceleration cutoff energy. Pohl & Esposito (1998) argued that if this injection electron index of 2.0 is employed, the EGRET excess above 1 GeV can be well explained by IC scattering.

At the higher energies of the TeV-PeV region, the diffuse gamma-ray emission was calculated by Berezinsky et al. (1993) in terms of cosmic-ray interaction with ISM, using the current models for high energy particle interaction. Assuming that the hadron spectral index is 2.15 (or 2.0) in SNRs, Berezhko & Völk (2000) showed that the averaged contribution to the diffuse gamma-ray flux should exceed the current model predictions (Hunter et al. 1997; Bertsch et al 1993) by a factor 5 (or 29) at 1 TeV.

Recently, upper limits for diffuse gamma-ray flux have been given by ground-based air shower arrays in the energy region 3 TeV to 1.4 PeV, and by imaging atmospheric Cherenkov telescopes (IACT) in the region above 500 GeV to above 1 TeV. In this paper we report new upper limits using the combined data with the Tibet-II and III arrays at 10 TeV.

2. EXPERIMENT

The Tibet-II array consists of 221 scintillation counters of 0.5 m^2 each, constructed at Yangbajing (4300 m a.s.l., 90.53°E, 30.11°N) in 1994, keeping the same lattice interval of 15 m as Tibet-I. The performance of the Tibet-II array is almost same as the Tibet-I which is described elsewhere (Amenomori et al. 1992, 1993). The mode energy is 10 TeV for air showers with $\Sigma\rho_{PT} \geq 15$ m^{-2}, where $\Sigma\rho_{PT}/2$ is the sum of the number of particles that hit all 0.5 m^2 detectors. The angular resolution is determined to be 0.9° at 10 TeV, calibrated by using the deficit shape of the Moon shadow (Amenomori et al. 1993, 1996).

In 1999, the array was enlarged in order to make a high detector density array, Tibet-III, with 533 scintillation counters and a 7.5 m lattice interval as shown in Fig. 2. In this figure detectors shown by open squares are excluded so as to keep a similar performance to the Tibet-II with respect to the mode energy and angular resolution. The performance and number of events obtained for these two arrays are given in Table 1.

Figure 3 shows an exposure map in galactic coordinates for air showers obtained with the Tibet-III array, with zenith angles $\theta \leq 50°$. The shower event density increases from light blue to dark blue. The Tibet-II array data produce a quite similar map. For the on-plane data, shower events are employed in the sky regions of $20° \leq l \leq 55°$ for the inner Galaxy (IG) and of $140° \leq l \leq 225°$ for the outer Galaxy (OG), in $|b| \leq 2°$ along the Galactic plane.

TABLE 1 .
ARRAY PERFORMANCE AND OBTAINED DATA

Fig. 1.— Map of the Tibef-II array at Yangbajing. Air shower events hitting the inner area with 15m detector distance are used in the analysis.

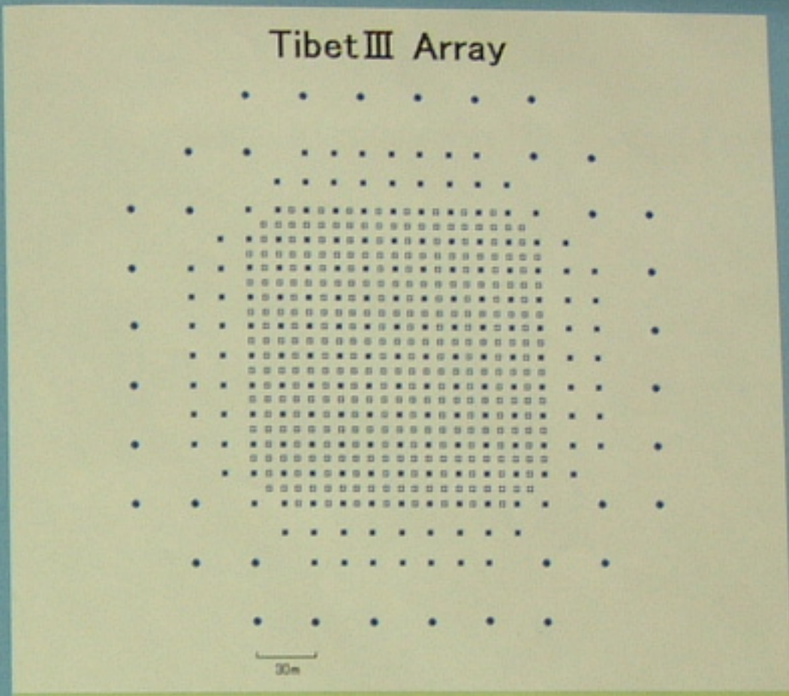

Fig. 2.— Map of the Tibet-III array at the status in 1999-02. Air shower events hitting the inner area with 7.5m detector distance are used in the analysis. But, the detectors shown by open squares are excluded so as to keep the same array condition as the Tibet-II.

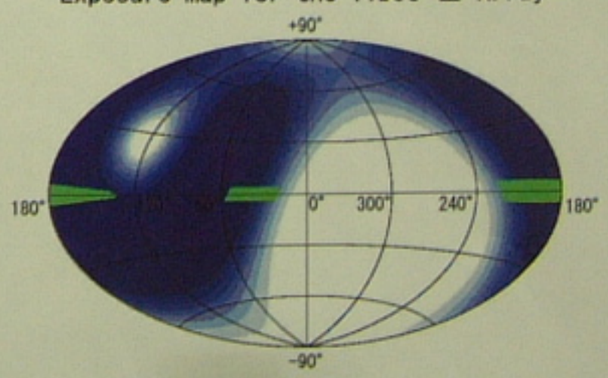

Fig. 3.— Tibet-III exposure map in the galactic coordinates for showers with zenith angles $\theta \leq 50°$. The event density increases from light blue to dark blue. The searched sky regions for diffuse gamma rays from the Galactic plane are indicated by narrow green ($|b| \leq 2°$) along the Galactic plane.

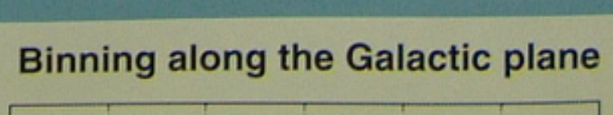

all 0.5 m^2 detectors. The angular resolution is determined to be 0.9° at 10 TeV, calibrated by using the deficit shape of the Moon shadow (Amenomori et al. 1993, 1996).

In 1999, the array was enlarged in order to make a high detector density array, Tibet-III, with 533 scintillation counters and a 7.5 m lattice interval as shown in Fig. 2. In this figure detectors shown by open squares are excluded so as to keep a similar performance to the Tibet-II with respect to the mode energy and angular resolution. The performance and number of events obtained for these two arrays are given in Table 1.

Figure 3 shows an exposure map in galactic coordinates for air showers obtained with the Tibet-III array, with zenith angles $\theta \leq 50°$. The shower event density increases from light blue to dark blue. The Tibet-II array data produce a quite similar map. For the on-plane data, shower events are employed in the sky regions of $20° \leq l \leq 55°$ for the inner Galaxy (IG) and of $140° \leq l \leq 225°$ for the outer Galaxy (OG), in $|b| \leq 2°$ along the Galactic plane.

TABLE 1 .
ARRAY PERFORMANCE AND OBTAINED DATA

Air Shower Array	Lattice Interval (m)	Inner Area (m^2)	Trigg Rate† (Hz)	Observd Period Net days	Pre-analysis for $\Sigma\rho_{PT} \geq 15$ Events (10^9)	E_{mode} (TeV)	Ang. res. (deg.)	Inner Events (10^9)
Tibet-II	15	28,350	200	1997 Feb ~99 Sep 551.2	5.44	10	0.9	4.14
Tibet-III	7.5	(21,300*)	680	1999 Nov ~01 Oct 517.3	4.08	10	0.9	2.49

† Trigger level is any four detectors with 0.80 particles per detector.
* At the status in 1999~2002.

3. DATA ANALYSIS

For the present analysis at around 10 TeV, 2.49 $\times 10^9$ events which hit the inner area of the Tibet-III are added to the last analysis (Amenomori et al. 2002) of 4.14 $\times 10^9$ events obtained with the Tibet-II both with the zenith angles $\theta \leq 50°$, as tabulated in Table 1. Those air shower events are assigned to the sky regions from which they arrived, of 4.5° (5.625°) bin 80 (64) belts along the Galactic plane of the inner (outer) Galaxy in equatorial coordinates both for the Tibet-II and III array data, as shown in Fig. 4. This figure shows 4.5° bin warped belts for IG with the declination range of $-10° \leq \delta \leq 20°$ and 5.625° bin warped belts for OG with $-10° \leq \delta \leq 60°$. These declination ranges of the on-plane belts in the equatorial coordinates correspond to parts of a convex lens shape, with an average thickness of 4° in galactic coordinates, as shown in Fig. 2.

The primary reason those warped belts are employed is to detect gamma-ray signals as accurately as possible if they are emitted from the Galactic plane with greater intensity than from other sky regions. In addition, the zenith angle distribution, and hence the primary energies of detected air showers are quite similar in each warped belt. This is very important when we estimate the on-plane background intensity at the same energy for both the on-plane and many off-plane belts, because the gamma-ray energy spectrum is still unknown. The final reason is that the background estimate, especially for the OG, is little affected by the IG plane, because the warped belts crossing the IG plane do so diagonally, over a narrow band of longitudes.

Figure 5 shows the distribution of the number of events in 4.5° bin warped belts. The abscissa represents the right ascension of each warped belt at the declination 30°, which is the same as the latitude of the Yangbajing site. The solid lines are the curves fitted to the experimental data, ignoring the on-plane data. In this figure, the cases for (a) IG and (b) OG at 10 TeV are shown in the 4.5° and 5.625° bin analysis, respectively. The anisotropy

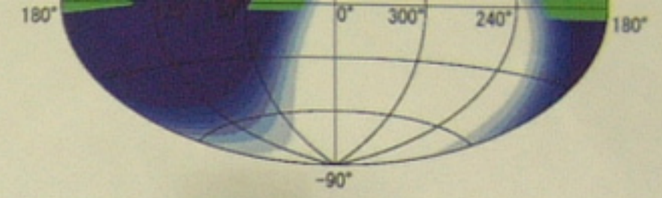

Fig. 3.— Tibet-III exposure map in the galactic coordinates for showers with zenith angles $\theta \leq 50°$. The event density increases from light blue to dark blue. The searched sky regions for diffuse gamma rays from the Galactic plane are indicated by narrow green ($|b| \leq 2°$) along the Galactic plane.

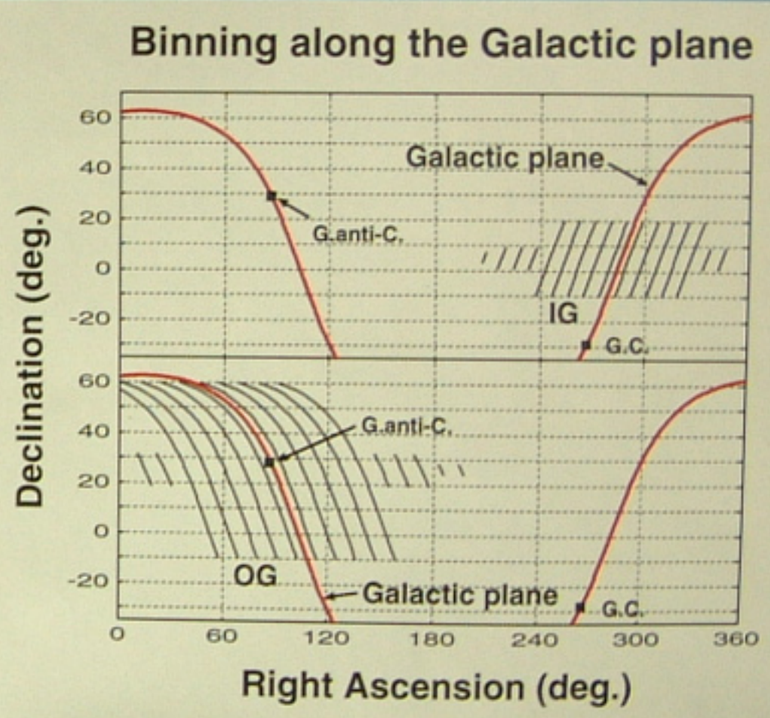

Fig. 4.— Warped belts of 4.5° width in the right ascension along the Galactic plane for IG (upper half) near the Galactic center and 5.625° width for OG (lower half) including the Galactic anticenter. Average thickness of the on-plane is about 4° both for IG and OG in galactic coordinates. These binnings of warped belts along the Galactic plane keep the quite same zenith angle distribution of detected air showers. Then, it assures the same average energy of primary gamma rays in each bin.

In order to see the adequacy of the fitting and on-plane excess in more detail, smaller ranges of the right ascension band of about 60° around the Galactic plane are shown in Fig. 7, where subfigures (a) and (b) correspond to those in Fig. 5. In each subfigure, the on-plane and off-plane data are indicated by filled circles and filled triangles, respectively, and the blank squares indicate the data points excluded from the background estimation. Error bars are statistical only.

4. RESULTS

(3.625°) bin 80 (64) belts along the Galactic plane of the inner (outer) Galaxy in equatorial coordinates both for the Tibet-II and III array data, as shown in Fig. 4. This figure shows 4.5° bin warped belts for IG with the declination range of $-10° \leq \delta \leq 20°$ and 5.625° bin warped belts for OG with $-10° \leq \delta \leq 60°$. These declination ranges of the on-plane belts in the equatorial coordinates correspond to parts of a convex lens shape, with an average thickness of 4° in galactic coordinates, as shown in Fig. 2.

The primary reason those warped belts are employed is to detect gamma-ray signals as accurately as possible if they are emitted from the Galactic plane with greater intensity than from other sky regions. In addition, the zenith angle distribution, and hence the primary energies of detected air showers are quite similar in each warped belt. This is very important when we estimate the on-plane background intensity at the same energy for both the on-plane and many off-plane belts, because the gamma-ray energy spectrum is still unknown. The final reason is that the background estimate, especially for the OG, is little affected by the IG plane, because the warped belts crossing the IG plane do so diagonally, over a narrow band of longitudes.

Figure 5 shows the distribution of the number of events in 4.5° bin warped belts. The abscissa represents the right ascension of each warped belt at the declination 30°, which is the same as the latitude of the Yangbajing site. The solid lines are the curves fitted to the experimental data, ignoring the on-plane data. In this figure, the cases for (a) IG and (b) OG at 10 TeV are shown in the 4.5° and 5.625° bin analysis, respectively. The anisotropy of cosmic-ray intensity seen in this figure, with an amplitude of less than ±1%, is mainly due to some seasonal long suspensions of operation for construction and system calibration of the array.

An excess of the on-plane data over the fitted curve would be considered to be a gamma-ray signal, which is measured by a standard deviation of the number of showers, in two 2.25° (IG) or three 1.875° (OG) bin belts, by the formula $(E-B)/\sqrt{B}$, where E is the number of on-plane events and B is the estimated number of background events in the on-plane region. B is estimated from the solid curve which is obtained by the fitting of many off-plane belts, ignoring the central 13.5° width for IG and 13.125° ($-8.4375° \leq b \leq 4.6875°$) for OG. We intend to deduce the number of on-plane background events as accurately as possible from this fitted curve of the off-plane data. The solid curves in Figures 5(a) and (b) are assumed to show the number of the galactic cosmic rays.

Figure 6 shows the deviation distributions of the number of events from the fitted curves (the solid ones in Fig. 5) in (a) 2.25° for IG and (b) 1.875° bin off-plane belts for OG. Here, the abscissa represents a significance in the 2.25° (IG) or 1.875° (OG) bin off-plane belts. The solid curves are best-fit Gaussians with standard deviations of 0.897 and 1.042, respectively, and where data on the 13.5° or 13.1° width around the Galactic plane are excluded. Each standard deviation is almost equal in unity, although 0.897 for IG is not yet so good, the solid curves are considered to be fitted to the experimental data. Thus, we can accurately estimate the number of on-plane background events.

The diffuse gamma-ray intensity from the OG plane is likely to be much lower than that from the IG plane. The Crab Nebula, is located at $\alpha = 83.^{\circ}38', \delta = 22.^{\circ}01'$ ($l = 184.56°, b = -5.78°$) with a real angle distance of 5.78° from the central sheet of the OG plane. In order to diminish the influence of the Crab, seven warped belts of 1.875° width are omitted from the off-plane region. As a result, the real angle distance of the Crab is 3.56° from the on-plane region and 2.47° from the defined off-plane region. Therefore, the Crab is located sufficiently far from both the on-plane and off-plane regions, because the angular resolution of the Tibet-II and III is about 0.9° at 10 TeV.

Fig. 4.— Warped belts of 4.5° width in the right ascension along the Galactic plane for IG (upper half) near the Galactic center and 5.625° width for OG (lower half) including the Galactic anticenter. Average thickness of the on-plane is about 4° both for IG and OG in galactic coordinates. These binnings of warped belts along the Galactic plane keep the quite same zenith angle distribution of detected air showers. Then, it assures the same average energy of primary gamma rays in each bin.

In order to see the adequacy of the fitting and on-plane excess in more detail, smaller ranges of the right ascension band of about 60° around the Galactic plane are shown in Fig. 7, where subfigures (a) and (b) correspond to those in Fig. 5. In each subfigure, the on-plane and off-plane data are indicated by filled circles and filled triangles, respectively, and the blank squares indicate the data points excluded from the background estimation. Error bars are statistical only.

4. RESULTS

The significance of an on-plane excess, $(E-B)/\sqrt{B}$ measured in standard deviation of the number of on-plane events, is given in Table 2. No significant excess is found. We calculate the upper limits for the gamma-ray intensity using the methods given by Helene (1983) and Protheroe (1984) for a small excess or deficit on the Galactic plane. In this table, the flux ratio, $J_\gamma/J_{\rm CR}$, for 90% CL and 99% CL upper limits to the galactic cosmic rays is given at 10 TeV. The differential intensity multiplied by E^2 with these upper limits are also given, assuming gamma ray spectral index of 2.4, for the regions of IG ($20° \leq l \leq 55°$) and OG ($140° \leq l \leq 225°$) with $-2° \leq b \leq 2°$. A minor component of the isotropic diffuse gamma rays is included in the galactic cosmic rays because separating them is impossible in the Tibet air shower array due to the lack of any equipment to reduce the background hadron initiated air showers. In Table 2, the intensity upper limits are also given as 90% and 99% confidence level (CL), calculated from the above flux ratio and assuming a differential spectral index of 2.4 for the diffuse gamma rays, and using the all-particle energy spectrum of the galactic cosmic rays recently compiled by Apanasenko et al. (2001).

TABLE 2
LIMITS TO DIFFUSE GAMMA RAYS (Tibet II+III)

Inner or Outer Galactic Plane (Regions of l, b)	Significance (σ)	$1/\sqrt{B}$ at 10 TeV (10^{-4})	$\frac{J_\gamma(>E)}{J_{\rm CR}(>E)}$ at 10 TeV 90% CL (10^{-4})	99% CL (10^{-4})	$E^2\frac{dJ_\gamma(>E)}{dE}$ ($\rm cm^{-2}s^{-1}sr^{-1}MeV$) 90% CL ($10^{-3}$)	99% CL (10^{-3})
I G ($20° \leq l \leq 55°$) ($-2° \leq b \leq 2°$)	+1.27	0.56	4.83	6.73	2.0	2.8/4.05 = 0.7σ
O G ($140° \leq l \leq 225°$) ($-2° \leq b \leq 2°$)	-0.06	1.00	1.61	2.34	0.67	1.05/1.29 = 0.8σ

(Tibet II only)

tic Plane

Tibet, China

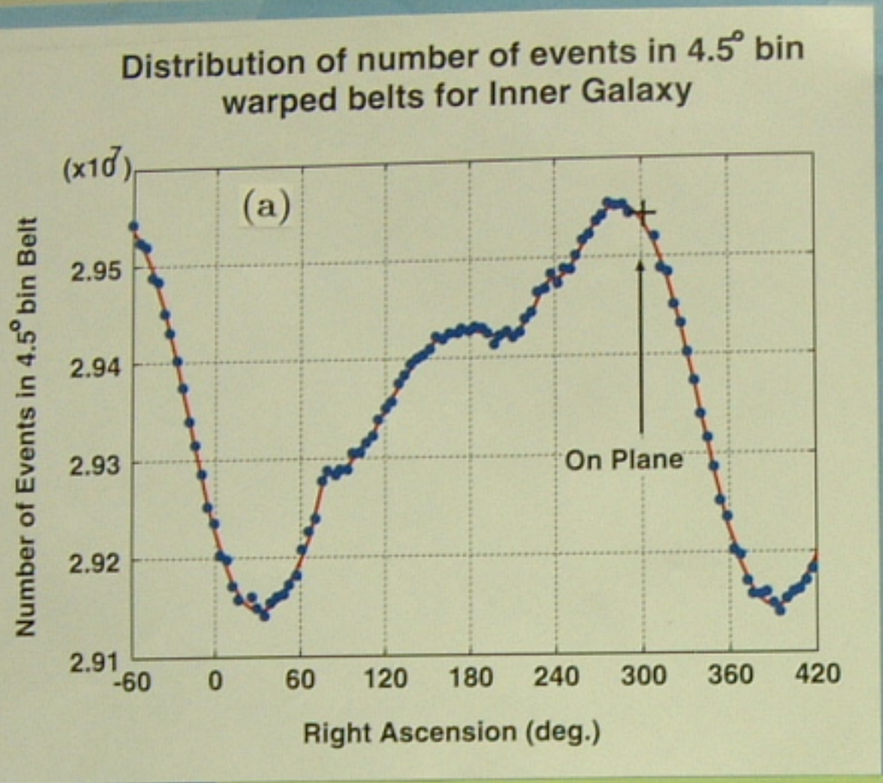

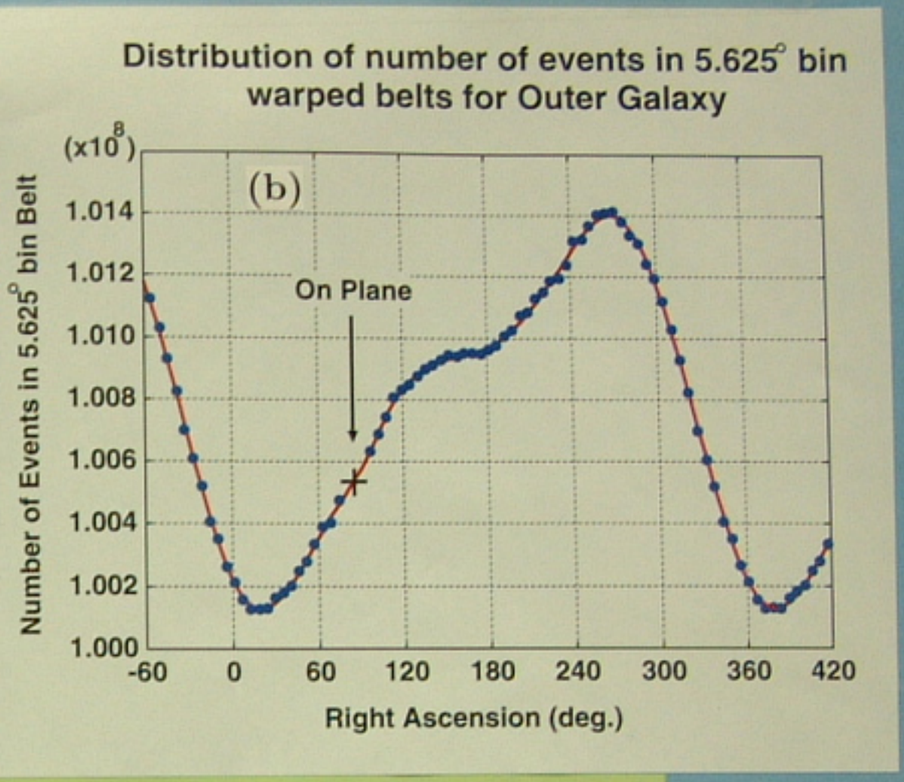

Fig. 5.— Distributions of number of events in 4° bin warped belts for (a) IG and (b) OG in Tibet-II + III data at 10 TeV. Abscissa represents the right ascension of each belt at the declination 30°. Solid red line are curves fitted to the experimental data. In each subfigure, the on-plane data point is shown by a large +.

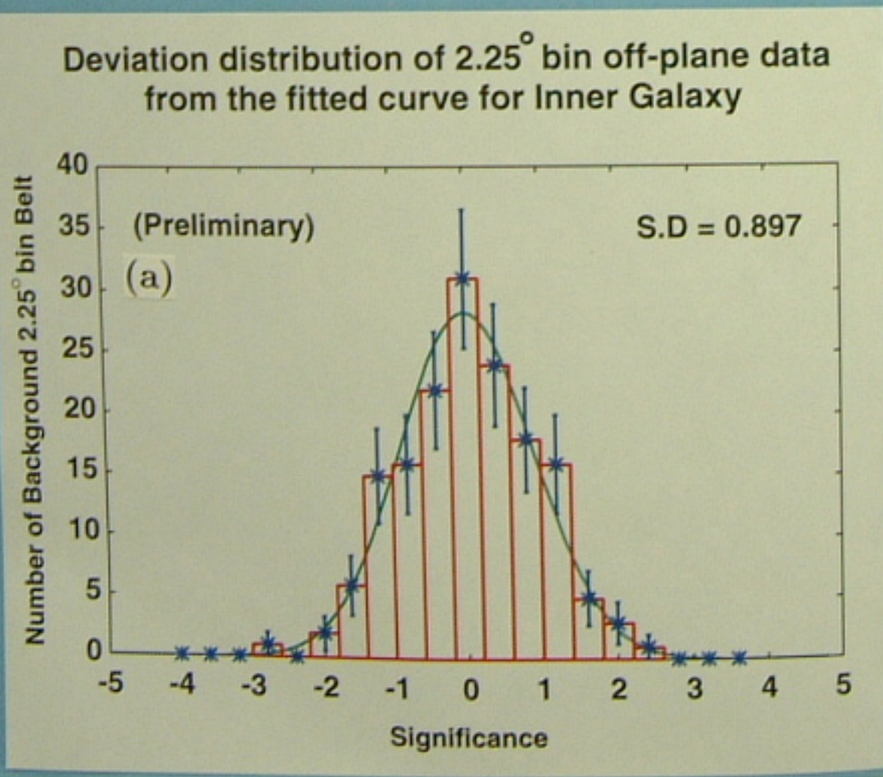

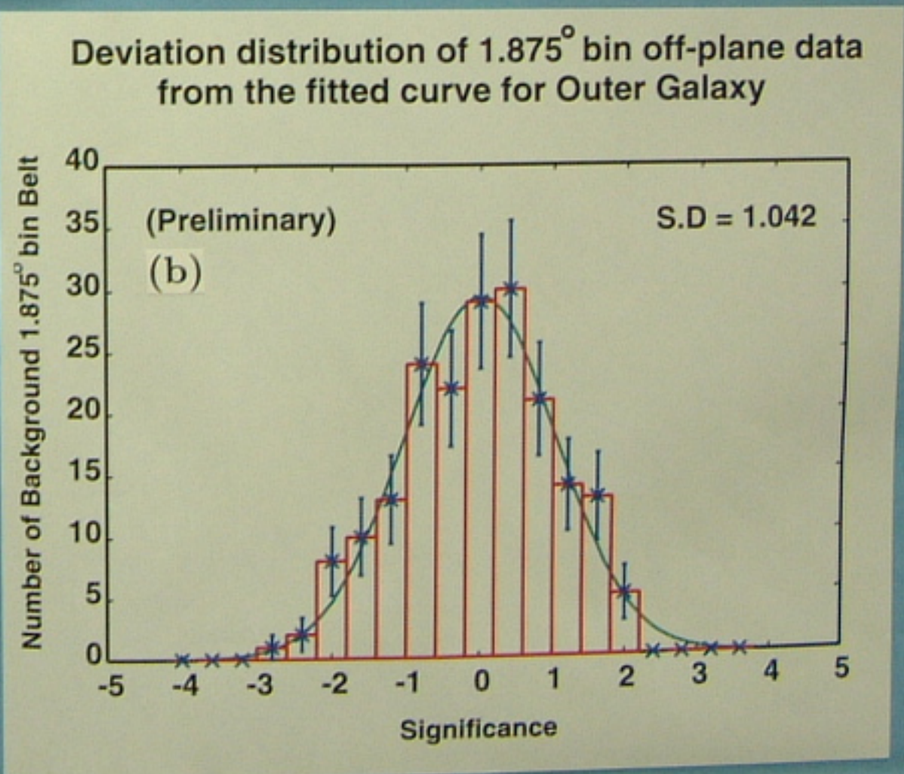

Fig. 6.— Deviation distributions of 2.25° bin IG (a) off-plane data and 1.875° bin OG (b) off-plane data from respective fitting curves at 10 TeV. For IG, the data in the central 13.5° are omitted from the off-plane data. For OG, the data in the range of $-8.4375° \leq b \leq 4.6875°$ (13.125° width) are also omitted to minimize the Crab's influence. Solid curves are best-fit Gaussians with a standard deviation designated in each subfigure.

Air shower
oe are used

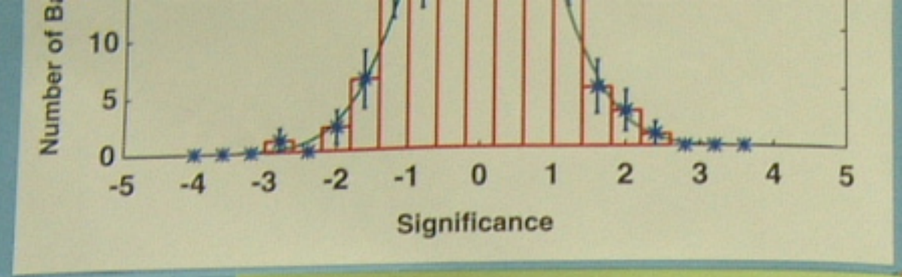

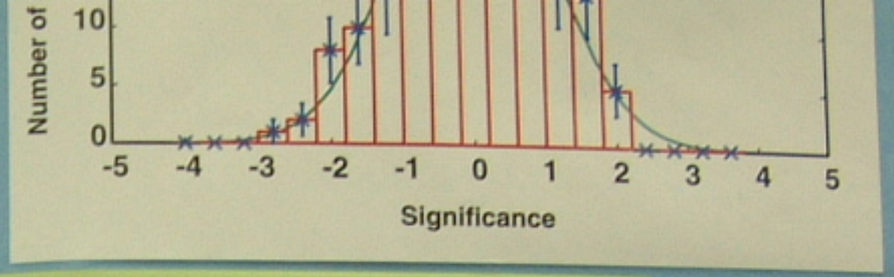

Fig. 6.— Deviation distributions of 2.25° bin IG (a) off-plane data and 1.875° bin OG (b) off-plane data from respective fitting curves at 10 TeV. For IG, the data in the central 13.5° are omitted from the off-plane data. For OG, the data in the range of $-8.4375° \leq b \leq 4.6875°$ (13.125° width) are also omitted to minimize the Crab's influence. Solid curves are best-fit Gaussians with a standard deviation designated in each subfigure.

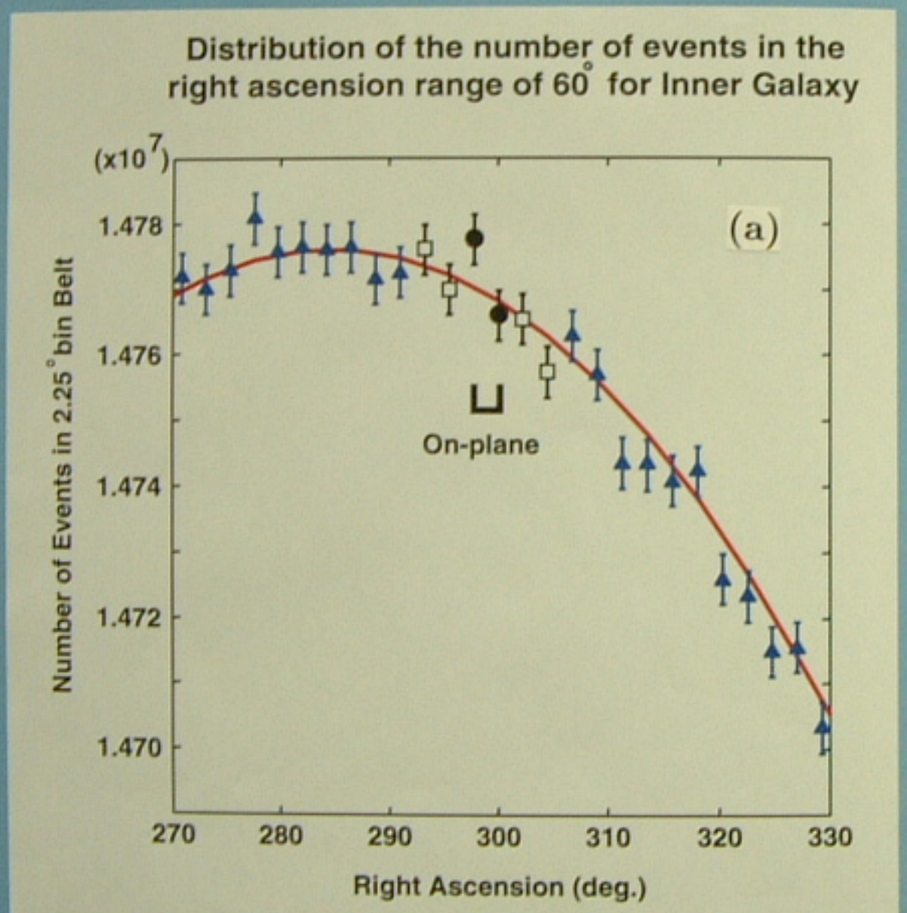

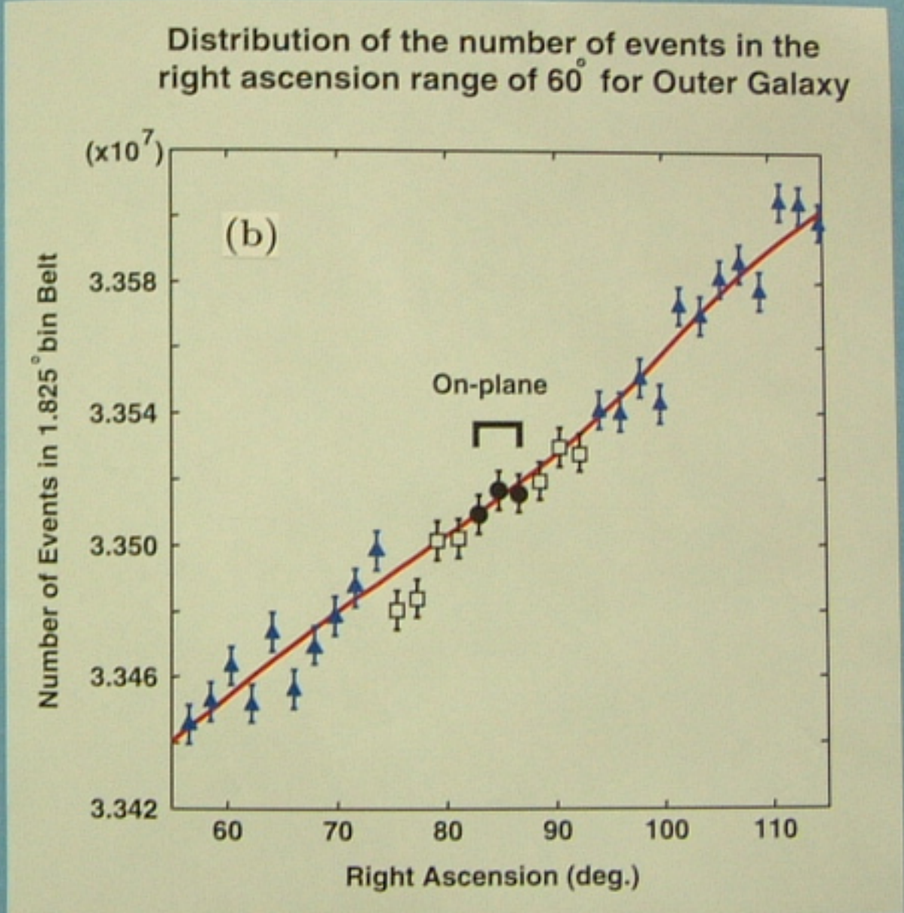

Fig. 7.— Distributions of the number of events in the right ascension range of 60°. Subfigures (a) and (b) correspond to those in Fig. 5. Abscissas are the same in Fig. 5. On-plane data are shown by filled circles, off-plane data by filled triangles, and open squares indicate data omitted from the background estimation. The solid curves fitted to the triangle data in respective sub-figures are used for estimation of the number of on-plane background events B. $E - B$ is the excess number of events over the solid curves in the on-plane belts.

solid curves fitted to the triangle data in respective sub-figures are used for estimation of the number of on-plane background events B. $E - B$ is the excess number of events over the solid curves in the on-plane belts.

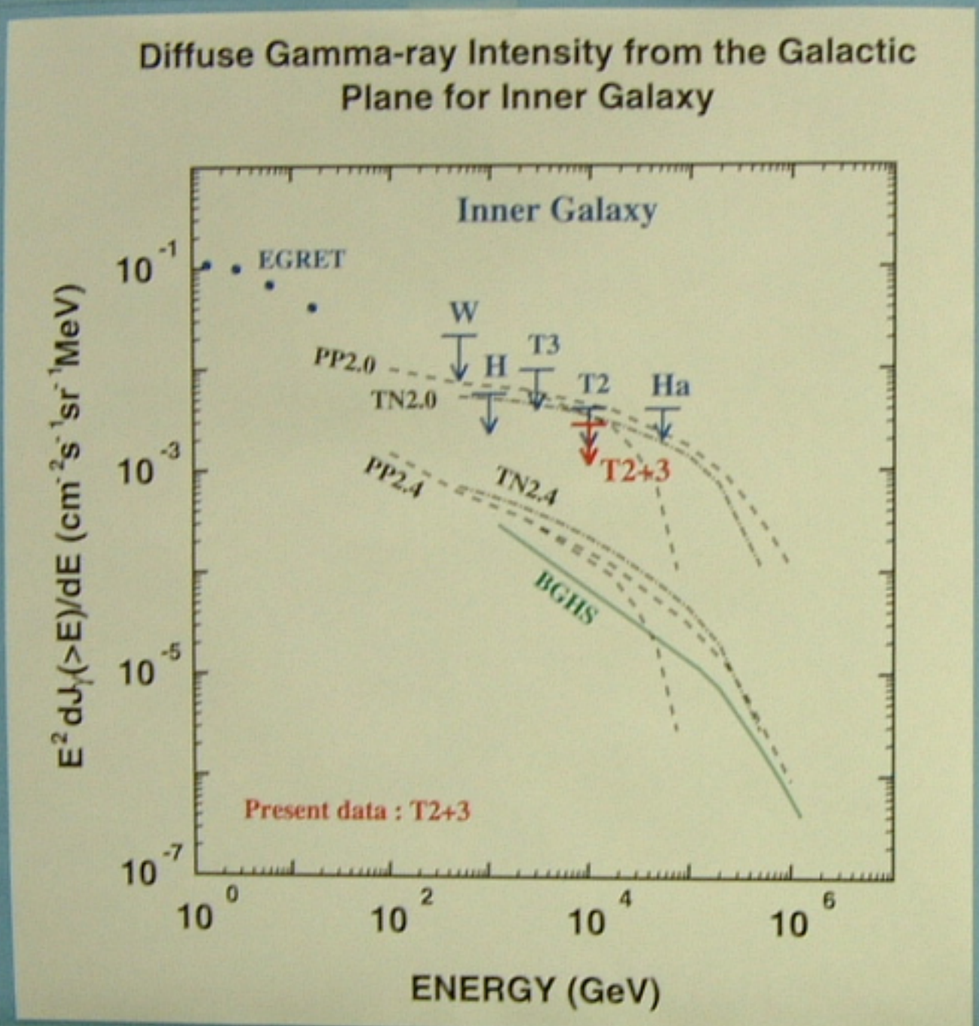

Fig. 8.— Diffuse gamma rays from the inner Galaxy (IG). Present result is labeled by T2+3 as 99% CL upper limits with red arrow, assuming a gamma-ray spectral index 2.4. T2 and T3 are the recent Tibet 99% CL upper limits at energy 10 TeV and 3 TeV (Amenomori et al. 2002). W and H indicate the Whipple's 99.9% CL (LeBohec et al. 2000) and HEGRA's 99% CL (Aharonian et al. 2001) upper limits with IACT. Ha is HEGRA Airobicc's 90% CL (Aharonian et al. 2002) upper limit. Theoretical curves are labeled by initials of the authors names. BGHS represents $\pi^\circ \rightarrow 2\gamma$ by Berezinsky et al. (1993). PP and TN are given by Porter & Protheroe (1997) and Tateyama & Nishimura (2001) for the inverse Compton. The numerals 2.0 or 2.4 following PP and TN indicate the electron source differential spectral indices.

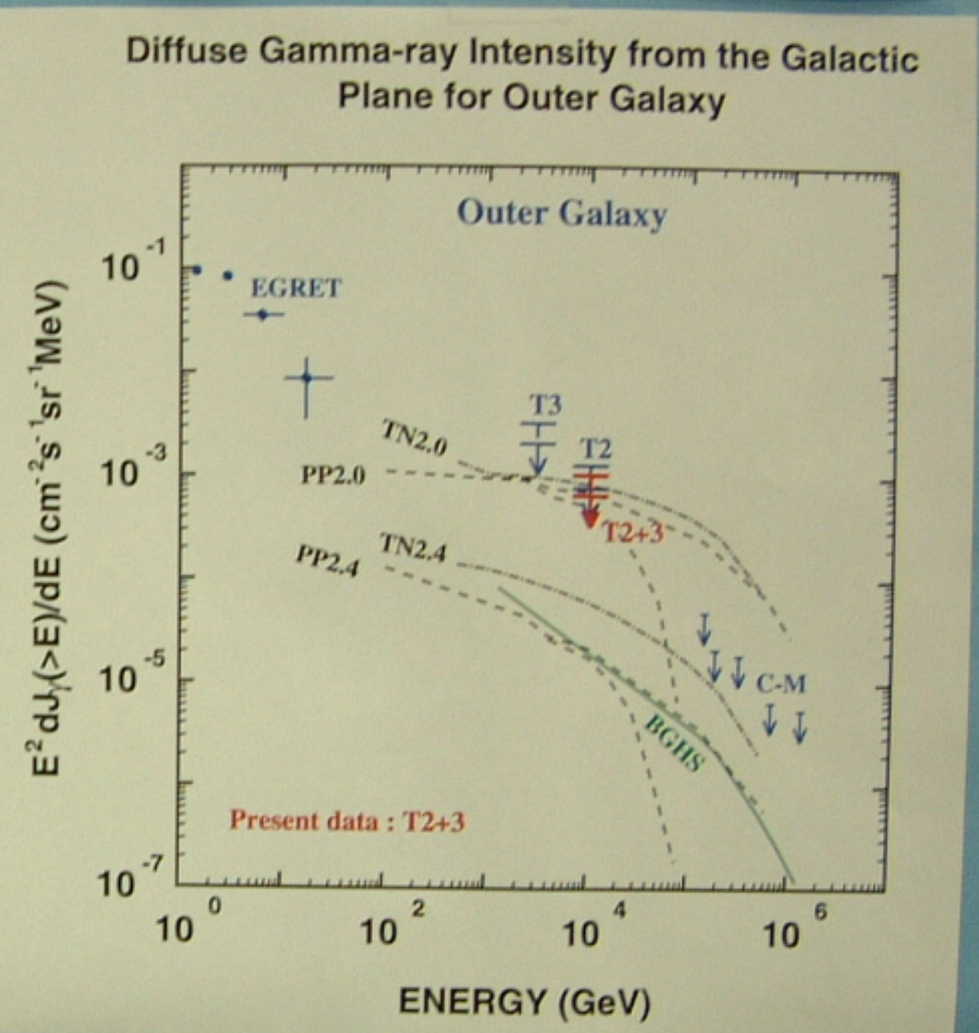

Fig. 9.— Diffuse gamma rays from the outer Galaxy (OG). Present data are labeled by T2+3 as 99% CL (upper bar) and 90% CL (lower bar) upper limits, assuming the same spectral index 2.4. The latter are compared with CASA-MIA 90% CL upper limits (labeled by C-M), based on muon-poor air shower data (Borione et al. 1998). Theoretical curves and their labels are the same as in Fig. 8.

Figure 8 shows the 99% CL upper limits thus obtained for diffuse gamma rays from the inner Galactic plane, $20^\circ \leq l \leq 55^\circ$ and $|b| \leq 2^\circ$, at 10 TeV. In this figure the Tibet upper limits with 99% CL are plotted for the Tibet-II (T2) at 10 TeV and for the Tibet-III (T3) at 3 TeV (Amenomori et al. 2002) The EGRET data (Hunter et al. 1997), $315^\circ \leq l \leq 45^\circ$ and $|b| \leq 2^\circ$, and the Cherenkov data are also plotted, including Whipple's 99.9% CL upper limit above 500 GeV (LeBohec et al. 2000) at the region of $38.5^\circ \leq l \leq 41.5^\circ$ and $|b| \leq 2^\circ$, and HEGRA-IACT's 99% CL upper limit above 1 TeV (Aharonian et al. 2001).

This work is supported in part by Grants-in-Aid for Scientific Research on Priority Areas from the Ministry of Education, Culture, Sports, Science and Technology in Japan and from the Committee of the Natural Science Foundation and the Academy of Sciences in China.

REFERENCES

gamma-ray spectral index 2.4. T2 and T3 are the recent Tibet 99% CL upper limits at energy 10 TeV and 3 TeV (Amenomori et al. 2002). W and H indicate the Whipple's 99.9% CL (LeBohec et al. 2000) and HEGRA's 99% CL (Aharonian et al. 2001) upper limits with IACT. Ha is HEGRA Airobicc's 90% CL (Aharonian et al. 2002) upper limit. Theoretical curves are labeled by initials of the authors names. BGHS represents $\pi^\circ \rightarrow 2\gamma$ by Berezinsky et al. (1993). PP and TN are given by Porter & Protheroe (1997) and Tateyama & Nishimura (2001) for the inverse Compton. The numerals 2.0 or 2.4 following PP and TN indicate the electron source differential spectral indices.

Figure 8 shows the 99% CL upper limits thus obtained for diffuse gamma rays from the inner Galactic plane, $20^\circ \leq l \leq 55^\circ$ and $|b| \leq 2^\circ$, at 10 TeV. In this figure the Tibet upper limits with 99% CL are plotted for the Tibet-II (T2) at 10 TeV and for the Tibet-III (T3) at 3 TeV (Amenomori et al. 2002) The EGRET data (Hunter et al. 1997), $315^\circ \leq l \leq 45^\circ$ and $|b| \leq 2^\circ$, and the Cherenkov data are also plotted, including Whipple's 99.9% CL upper limit above 500 GeV (LeBohec et al. 2000) at the region of $38.5^\circ \leq l \leq 41.5^\circ$ and $|b| \leq 2^\circ$, and HEGRA-IACT's 99% CL upper limit above 1 TeV (Aharonian et al. 2001) in a similar region of $38^\circ \leq l \leq 43^\circ$ and $|b| \leq 2^\circ$. Futher, the recent result by HEGRA AIROBICC's 90% CL upper limit (Aharonian et al. 2002) at several tens TeV is plotted. The theoretical curve calculated by Berezinsky et al. (1993) for $\pi^\circ \rightarrow 2\gamma$ due to the collision of cosmic-ray hadrons with ISM is drawn by a solid curve (BGHS) which is for the region of $20^\circ \leq l \leq 55^\circ$ and $|b| \leq 2^\circ$, deduced from their original paper.

For inverse Compton gamma rays calculated by Porter & Protheroe (1997) is shown by dashed curves for source electron spectral indices of 2.0 (PP2.0) and 2.4 (PP2.4) in the direction $l = 0^\circ$ and $b = 0^\circ$, the Galactic center. Similar theoretical curves calculated by Tateyama & Nishimura (2001) are shown by dot-dashed lines with source spectral indices of 2.0 (TN2.0) and 2.4 (TN2.4) in the direction $l = 0^\circ$ and $|b| \leq 2^\circ$. The density distribution of ISPF in their calculations is based on the compilations by Bloemen (1985) and Mathis et al. (1983). The present Tibet data at 10 TeV give the most stringent upper limit for the IC model with a source electron spectral index of 2.0.

Figure 9 shows the present results as 99% CL upper limits (upper bar of T2+3) for OG, $140^\circ \leq l \leq 225^\circ$ and $|b| \leq 2^\circ$, at 10 TeV. In this figure the Tibet-II (T2) at 10 TeV and Tibet-III (T3) at 3 TeV are also shown (Amenomori et al. 2002). The 90% CL upper limits (lower bars) are compared with the CASA-MIA 90% CL upper limits, which are based upon muon-poor air showers (Borione et al. 1998) at about 140 TeV-1.3 PeV, from the OG plane of $50^\circ \leq l \leq 200^\circ$ and $|b| \leq 2^\circ$. The CASA-MIA data can rule out the IC model with index 2.0 without acceleration energy cutoff, but can not rule out the case with an energy cutoff at 100 TeV. The theoretical curve by Berezinsky et al. (1993) is also shown for $\pi^\circ \rightarrow 2\gamma$ component (BGHS) in the region of $140^\circ \leq l \leq 225^\circ$ and $|b| \leq 2^\circ$. The IC gamma rays calculated by Porter & Protheroe (1996) for the region $50^\circ \leq l \leq 200^\circ$ and $|b| \leq 10^\circ$ for source spectral indices of 2.0 (PP2.0) and 2.4 (PP2.4) are shown, as well as the ones by Tateyama & Nishimura (2001) in the region of $l = 180^\circ$ and $|b| \leq 2^\circ$ for source spectral indices of 2.0 (TN2.0) and 2.4 (TN2.4). The present data are not sufficient to rule out the IC model with a spectral index of 2.0.

limits, assuming the same spectral index 2.4. The latter are compared with CASA-MIA 90% CL upper limits (labeled by C-M), based on muon-poor air shower data (Borione et al. 1998). Theoretical curves and their labels are the same as in Fig. 8.

This work is supported in part by Grants-in-Aid for Scientific Research on Priority Areas from the Ministry of Education, Culture, Sports, Science and Technology in Japan and from the Committee of the Natural Science Foundation and the Academy of Sciences in China.

REFERENCES

Aharonian, F.A. et al. 2001, A&A, 375, 1008

Aharonian, F.A. et al. 2002, Astropart. phys., 17, 459

Amenomori, M. et al. 1992, Phys. Rev. Letters, 69, 2468

———. 1993, Phys. Rev. D, 47, 2675

———. 1996, ApJ, 464, 954

———. 2002, ApJ, 480, in press

Apanasenko, A.V. et al. 2001, Astropart. Phys., 16, 13

Berezhko, E.G., & Völk, H.J. 2000, ApJ, 540, 923

Berezinsky, V.S., Gaisser, T.K., Halzen, F., & Stanev, T. 1993, Astropart. Phys., 1, 281

Bertsch, D.L. et al. 1993, ApJ, 416, 587

Bloemen, J.B.G.M. 1985, A&A, 145, 391

Borione, A. et al. 1998, ApJ, 493, 175 H. 1948, Phys. Rev., 73, 449

Hunter, S.D. et al. 1997, ApJ, 481, 205

LeBohec, S. et al. 2000, ApJ, 539, 209

Mathis, J.S., Mezger, P.G., & Panagia, N. 1983, A&A, 128, 212

Mori, S. 1997, ApJ, 478, 225

Pohl, M., & Esposito, J.A. 1998, ApJ, 507, 327

Porter, T.A., & Protheroe, R.J. 1997, J. Phys. G, 23, 1765

Tateyama, N., & Nishimura, J. 2001, Proc. 27th Int. Cosmic Ray Conf. (Hamburg), 6, 2343; in this Symposium

Webber, W.R. 1999, Proc. 26th Int. Cosmic Ray Conf. (Salt Lake City), 4, 97